

Accurate characterization of the stellar and orbital parameters of the exoplanetary system WASP-33 b from orbital dynamics

L. Iorio¹★

¹*I Ministero dell’Istruzione, dell’Università e della Ricerca (M.I.U.R.), Viale Unità di Italia 68 Bari, (BA) 70125, Italy*

20 June 2022

ABSTRACT

By using the most recently published Doppler tomography measurements and accurate theoretical modeling of the oblateness-driven orbital precessions, we tightly constrain some of the physical and orbital parameters of the planetary system hosted by the fast rotating star WASP-33. In particular, the measurements of the orbital inclination i_p to the plane of the sky and of the sky-projected spin-orbit misalignment λ at two epochs six years apart allowed for the determination of the longitude of the ascending node Ω and of the orbital inclination I to the apparent equatorial plane at the same epochs. As a consequence, average rates of change $\dot{\Omega}_{\text{exp}}$, \dot{I}_{exp} of these two orbital elements, accurate to a $\approx 10^{-2}$ deg yr⁻¹ level, were calculated as well. By comparing them to general theoretical expressions $\dot{\Omega}_{J_2}$, \dot{I}_{J_2} for their precessions induced by an oblate star whose symmetry axis is arbitrarily oriented, we were able to determine the angle i^* between the star’s spin S and the line of sight and its first even zonal harmonic J_2^* obtaining $i^* = 37.8_{-10.8}^{+10.1}$ deg, $J_2^* = (2.1_{-0.8}^{+0.5}) \times 10^{-4}$. As a by-product, the angle between S and the orbital angular momentum \mathbf{L} is as large as about $\psi \approx 100$ deg ($\psi^{2008} = 99.4_{-3.9}^{+5.5}$ deg, $\psi^{2015} = 102.7_{-3.9}^{+5.2}$ deg), and changes at a rate $\dot{\psi} = 0.506_{-1.58}^{+1.52}$ deg yr⁻¹. The predicted general relativistic Lense-Thirring precessions, of the order of $\approx 10^{-3}$ deg yr⁻¹, are, at present, about one order of magnitude below the measurability threshold.

Key words: stars: planetary systems–gravitation–celestial mechanics

1 INTRODUCTION

Steady observations of a test particle orbiting its primary over time intervals much longer than its orbital period P_b can reveal peculiar cumulative features of its orbital motion which may turn out as valuable tools to either put to the test fundamental theories or characterize the physical properties of the central body acting as source of the gravitational field. It has been just the case so far in several different astronomical and astrophysical scenarios ranging, e.g., from the early pioneering determinations of the multipole moments of the non-central gravitational potential of the Earth with artificial satellites (Kozai 1961; King-Hele 1962; Cook 1962) to the celebrated corroborations of the Einsteinian General Theory of Relativity (GTR) with the explanation of the anomalous (at that time) perihelion precession of Mercury (Einstein 1915)-observationally known since decades (Le Verrier 1859)-, several binary systems hosting at least one emitting pulsar (Hulse & Taylor 1975; Burgay et al. 2003; Lyne et al. 2004; Kramer et al. 2006), and Earth’s satellites (Lucchesi & Peron 2010, 2014) implementing earlier ideas put forth since the dawn of the space era and beyond (Lapaz 1954; Cugusi & Proverbio 1978). Plans exist to use in a similar way the stars revolving around the supermassive black hole in Sgr A* (Ghez et al.

2008; Gillessen et al. 2009; Angélib, Saha & Merritt 2010; Zhang, Lu & Yu 2015).

With over¹ 1500 planets discovered so far and counting (Han et al. 2014), most of which orbiting very close to their parent stars (Howard 2013), extrasolar systems (Perryman 2014), in principle, represent ideal probes to determine or, at least, constrain some physical parameters of their stellar partners through their orbital dynamics. One of them is the quadrupole mass moment J_2 , accounting for the flattening of the star. It is connected with fundamental properties of the stellar interior such as, e.g., the non-uniform distribution for both velocity rates and mass (Rozelot, Damiani & Pireaux 2009; Damiani et al. 2011; Rozelot & Damiani 2011; Rozelot & Fazel 2013). Also GTR may turn out a valuable goal for exoplanets’ analysts also from a practical point of view. Indeed, by assuming its validity, it may be used as a tool for dynamically characterizing the angular momentum S of the host stars via the so-called Lense-Thirring effect (Lense & Thirring 1918). Such a dynamical variable is able to provide relevant information about the inner properties of stars and their activity. Furthermore, it plays the role of an important diagnostic for putting to the test theories of stellar formation. The angular momentum can also have a crucial

★ E-mail: lorenzo.iorio@libero.it

¹ See, e.g., <http://exoplanets.org/> on the WEB.

impact in stellar evolution, in particular towards the higher mass (Tarañdar & Vardya 1971; Wolff, Edwards & Preston 1982; Vigneron et al. 1990; Wolff & Simon 1997; Herbst & Mundt 2005; Jackson, MacGregor & Skumanich 2005). As a naive measure of the relevance of the Einsteinian theory of gravitation in a given binary system characterized by mass M , proper angular momentum S and extension r , the magnitude of the ratios of some typical gravitational lengths to r can be assumed. By taking

$$r_M = \frac{GM}{c^2}, \quad (1)$$

$$r_S = \frac{S}{Mc}, \quad (2)$$

where G and c are the Newtonian gravitational constant and the speed of light in vacuum, respectively, it can be easily noted that, for exoplanets hosted by Sun-like stars at, say, $r = 0.005$ au, Eqs 1 to 2 yield

$$\frac{r_M}{r} = 2 \times 10^{-6}, \quad (3)$$

$$\frac{r_S}{r} = 4 \times 10^{-7}. \quad (4)$$

Such figures are substantially at the same level of, or even larger than those of the double pulsar (Burgay et al. 2003; Lyne et al. 2004; Kramer et al. 2006), for which one has

$$\frac{r_M}{r} = 4 \times 10^{-6}, \quad (5)$$

$$\frac{r_S}{r} = 8 \times 10^{-8}. \quad (6)$$

It shows that, in principle, some of the extrasolar planetary systems may well represent important candidates to perform also tests of relativistic orbital dynamics.

In the present work, we will deal with WASP-33 b (Collier Cameron et al. 2010). It is a planet closely transiting a fast rotating and oblate main sequence star along a circular, short-period ($P_b = 1.21$ d) orbit which is highly inclined to the stellar equator. In Iorio (2011b) it was suggested that, in view of the relatively large size of some classical and general relativistic orbital effects, they could be used to better characterize its parent star as long as sufficient accurate data records were available. It has, now, became possible in view of the latest Doppler tomography measurements processed by Johnson et al. (2015), and of more accurate theoretical models of the orbital precessions involved (Iorio 2011c, 2012).

The plan of the paper is as follows. In Section 2, we illustrate our general analytical expressions for the averaged classical and relativistic precessions of some Keplerian orbital elements in the case of an arbitrary orientation of the stellar symmetry axis and of an unrestricted orbital geometry. Section 3 describes the coordinate system adopted in this astronomical laboratory. Our theoretical predictions of the orbital rates of change are compared to the corresponding phenomenologically measured precessions in Section 4, where tight constraints on some key stellar parameters are inferred, and the perspectives of measuring the Lense-Thirring effect are discussed. Section 5 is devoted to summarizing our findings.

2 THE MATHEMATICAL MODEL OF THE ORBITAL PRECESSIONS

A particle at distance r from a central rotating body of symmetry axis direction $\hat{S} = \{\hat{S}_x, \hat{S}_y, \hat{S}_z\}$ experiences an additional non-central acceleration (Vrbik 2005)

$$\mathbf{A}_{J_2} = -\frac{3GMJ_2R^2}{2r^4} \left\{ \left[1 - 5(\hat{r} \cdot \hat{S})^2 \right] \hat{r} + 2(\hat{r} \cdot \hat{S}) \hat{S} \right\}, \quad (7)$$

which causes long-term orbital precessions. For a generic orientation of \hat{S} in a given coordinate system, they were analytically worked out by² Iorio (2011c). Among them³, we have

$$\begin{aligned} \dot{\Omega}_{J_2} = & \frac{3n_b J_2 R^2}{4a^2 (1-e^2)^2} \left\{ 2\hat{S}_z \cos 2I \csc I (\hat{S}_x \sin \Omega - \hat{S}_y \cos \Omega) + \right. \\ & \left. + \cos I [1 - 3\hat{S}_z^2 + (\hat{S}_y^2 - \hat{S}_x^2) \cos 2\Omega - 2\hat{S}_x \hat{S}_y \sin 2\Omega] \right\}, \quad (8) \end{aligned}$$

$$\begin{aligned} \dot{I}_{J_2} = & -\frac{3n_b J_2 R^2}{2a^2 (1-e^2)^2} (\hat{S}_x \cos \Omega + \hat{S}_y \sin \Omega) [\hat{S}_z \cos I + \\ & + \sin I (\hat{S}_x \sin \Omega - \hat{S}_y \cos \Omega)], \quad (9) \end{aligned}$$

which will be relevant for our purposes. In Eqs 8 to 9, a is the semimajor axis, $n_b = \sqrt{GMa^{-3}}$ is the Keplerian mean motion, e is the eccentricity, I is the inclination of the orbital plane with respect to the coordinate $\{x, y\}$ plane adopted, and Ω is the longitude of the ascending node counted in the $\{x, y\}$ plane from a reference x direction to the intersection of the orbital plane with the $\{x, y\}$ plane itself. Note that if the body's equatorial plane is assumed as $\{x, y\}$ plane, i.e. if $\hat{S}_x = \hat{S}_y = 0$, $\hat{S}_z = 1$, eq. (8) reduces to the well known expression

$$\dot{\Omega}_{J_2} = -\frac{3n_b J_2 R^2}{2a^2 (1-e^2)^2} \cos I; \quad (10)$$

with this particular choice, I coincides with the angle ψ between S and the particle's orbital angular momentum L . It is important to stress that, in the general case, the cumbersome multiplicative geometrical factor in Equation 8 depending on the spatial orientation of the orbit and of the spin axis does not reduce to $\cos \psi$, as it will explicitly turn out clear in Section 3. On the other hand, it can be easily guessed from the fact that $\cos \psi$ is linear in the components of \hat{S} , while the acceleration of Equation 7 is quadratic in them, whatever parametrization is adopted. Such an extrapolation of a known result valid only in specific cases is rather widespread in the literature (see, e.g., Iorio (2011b); Barnes et al. (2013); Johnson et al. (2015)), and may lead to errors when accurate results are looked for. Eqs 8 to 9 are completely general, and can be used with any coordinate system provided that the proper identifications pertaining the angular variables are made.

Here, we offer an alternative derivation of Eqs 8 to 9 with respect to the one in Iorio (2011c), which is based on the Gauss perturbative equations; instead, here we will use the Lagrange pertur-

² The replacement $Q_2 \rightarrow GMJ_2R^2$ must be done in the equations by Iorio (2011c) to obtain the present ones. Other conventions exist in the literature about dimensional quadrupole moments Q , mainly differing for the sign and the inclusion of G .

³ Also the argument of pericenter ω and the mean anomaly M are impacted by J_2 with long-term precessions. We will not display them here because they are not relevant in the present study.

bative scheme. The perturbing potential energy per unit mass due to the primary's oblateness is (Bertotti, Farinella & Vokrouhlick 2003)

$$\mathcal{R}_{J_2} = \frac{n_b^2 a^3}{r} J_2 \left(\frac{R}{r} \right)^2 P_2(\cos \delta), \quad (11)$$

where

$$P_2(\xi) = \frac{1}{2} (3\xi^2 - 1) \quad (12)$$

is the Legendre polynomial of degree 2, and δ is the angle between \hat{r} and \hat{S} . The acceleration, calculated as

$$\mathbf{A}_{J_2} = -\nabla \mathcal{R}_{J_2}, \quad (13)$$

agrees with Equation 7. From Equation 11, the average over one orbital revolution is obtained by evaluating it onto the unperturbed Keplerian ellipse and using, e.g., the true anomaly f as vast variable of integration. One gets

$$\begin{aligned} \langle \mathcal{R}_{J_2} \rangle_{P_b} &= \frac{1}{P_b} \int_0^{P_b} U_{J_2} dt = -\frac{J_2 n_b^2 R^2}{16(1-e^2)^{3/2}} \left[-1 + 3\hat{S}_z^2 + \right. \\ &+ (9\hat{S}_z^2 - 3) \cos 2I + 6(\hat{S}_z^2 + 2\hat{S}_y^2 - 1) \sin^2 I \cos 2\Omega + \\ &+ 12\hat{S}_z \sin 2I (\hat{S}_x \sin \Omega - \hat{S}_y \cos \Omega) - \\ &\left. - 12\hat{S}_x \hat{S}_y \sin^2 I \sin 2\Omega \right]. \end{aligned} \quad (14)$$

Note that, in the case $\hat{S}_x = \hat{S}_y = 0, \hat{S}_z = 1$, Equation 14 reduces to

$$\langle \mathcal{R}_{J_2} \rangle_{P_b} = -\frac{J_2 n_b^2 R^2}{8(1-e^2)^{3/2}} (1 + 3 \cos 2I), \quad (15)$$

in agreement with Equation (12.72) of Bertotti, Farinella & Vokrouhlick (2003). Finally, the Lagrange perturbative equations (Bertotti, Farinella & Vokrouhlick 2003) for the long-term precessions of Ω and I , averaged over one orbital period,

$$\dot{\Omega} = -\frac{1}{n_b a^2 \sqrt{1-e^2} \sin I} \frac{\partial \langle \mathcal{R} \rangle}{\partial I}, \quad (16)$$

$$\dot{I} = \frac{1}{n_b a^2 \sqrt{1-e^2} \sin I} \left(\frac{\partial \langle \mathcal{R} \rangle}{\partial \Omega} - \cos I \frac{\partial \langle \mathcal{R} \rangle}{\partial \omega} \right), \quad (17)$$

calculated with Equation 14, yield just Eqs 8 to 9.

The general relativistic gravitomagnetic field due to the angular momentum \mathbf{S} of the central body induces the Lense-Thirring effect (Lense & Thirring 1918), whose relevant orbital precessions, valid for an arbitrary orientation of \mathbf{S} , are⁴ (Iorio 2012)

$$\dot{\Omega}_S = \frac{2GS}{c^2 a^3 (1-e^2)^{3/2}} \left[\hat{S}_z + \cot I (\hat{S}_y \cos \Omega - \hat{S}_x \sin \Omega) \right], \quad (18)$$

$$\dot{I}_S = \frac{2GS}{c^2 a^3 (1-e^2)^{3/2}} (\hat{S}_x \cos \Omega + \hat{S}_y \sin \Omega). \quad (19)$$

The perspectives of detecting general relativity, mainly in its spin-independent, Schwarzschild-type manifestations, with exoplanets

⁴ The gravitomagnetic pericenter precession, not relevant for us here, will not be shown.

have been studies so far by several authors (Iorio 2006; Adams & Laughlin 2006a,b,c; Heyl & Gladman 2007; Pál & Kocsis 2008; Jordán & Bakos 2008; Ragozzine & Wolf 2009; Iorio 2011a,b; Harranas, Ragos & Mioc 2011; Xie & Deng 2014; Li 2012; Zhao & Xie 2013).

3 THE COORDINATE SYSTEM ADOPTED

For consistency reasons with the conventions adopted by Johnson et al. (2015), who, in turn, followed Queloz et al. (2000), the coordinate system used in the present analysis is as follows (see Figure 1). The line of sight, directed towards the observer, is assumed as reference y axis, while the z axis is determined by the projection of the stellar spin axis \hat{S} onto the plane of the sky. The x axis is straightforwardly chosen perpendicular to both the other two axes in such a way to form a right-handed coordinate system; thus, it generally does not point towards the Vernal Equinox ν at a reference epoch. Then, with the present choice, the coordinate $\{x, y\}$ plane does not coincide with the plane of the sky which, instead, is now spanned by the z and x axes; the $\{x, y\}$ plane is known as apparent equatorial plane (Queloz et al. 2000). The planetary longitude of the ascending node Ω lies in it, being counted from the x axis to the intersection of the orbital plane with the apparent equatorial plane itself; thus, in general, Ω does not stay in the plane of the sky. It is important since the values of the node reported in Table 1 of Johnson et al. (2015) refer just to this coordinate system. Moreover, with such conventions, the angle I between the orbital plane and the coordinate $\{x, y\}$ plane entering the precessional formulas of Eqs 8 to 19 is not the orbital inclination i_p , which refers the plane of the sky. Instead, I , which is also the angle between the planetary orbital angular momentum \mathbf{L} and the sky-projected stellar spin axis along the z axis, has to be identified with the angle α of Queloz et al. (2000). By thinking to it as a colatitude angle of \hat{L} in a spherical coordinate system, the components of the unit vector of the planetary orbital angular momentum are

$$\hat{L}_x = \sin I \sin \Omega, \quad (20)$$

$$\hat{L}_y = -\sin I \cos \Omega, \quad (21)$$

$$\hat{L}_z = \cos I. \quad (22)$$

Note that, in general, both I and Ω are not directly measurable. If i^* is the angle between \hat{S} and the line of sight, the components of the star's spin axis in our coordinate system are

$$\hat{S}_x = 0, \quad (23)$$

$$\hat{S}_y = \cos i^*, \quad (24)$$

$$\hat{S}_z = \sin i^*. \quad (25)$$

An angle which is measurable is the so-called projected spin-orbit misalignment λ . It lies in the plane of the sky, and is delimited by the projections of both the stellar spin axis and of the planetary orbital angular momentum. In our coordinate system, λ, i_p are the longitude and the colatitude spherical angles, respectively, with λ reckoned from the z axis to the projection of \hat{L} onto the plane of the sky. As such, the components of the planetary orbital angular

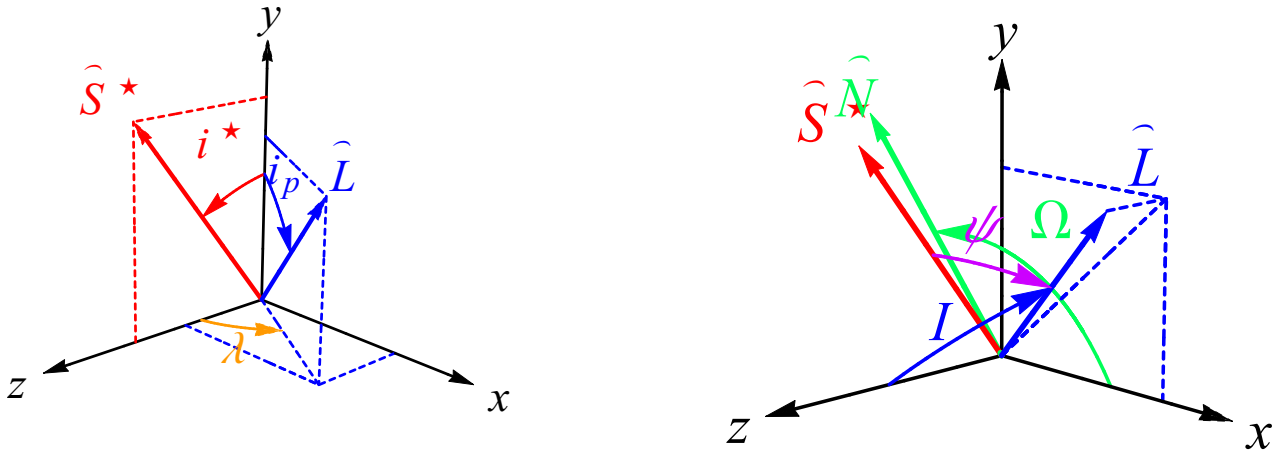


Figure 1. The coordinate system adopted. The axes x and z span the plane of the sky in such a way that the projection of the stellar spin axis S^* onto it defines the z axis. The y axis is directed along the line of sight towards the observer. The $\{x, y\}$ plane is the apparent equatorial plane. The inclination of the orbital plane to the plane of the sky is i_p , while i^* is the angle between the line of sight and the star's spin axis. The sky-projected spin-orbit misalignment angle λ lies in the plane of the sky, and is delimited by the projections of S^* and L onto it. The unit vector \hat{N} of the line of the nodes lies in the apparent equatorial plane perpendicularly to the projection of L onto it. The longitude of the ascending node Ω is counted in the $\{x, y\}$ plane from the x axis to the line of the nodes. The values of the angles were arbitrarily chosen just for illustrative purposes. The inclination of the orbital plane to the apparent equatorial plane is I . The angle between \hat{S}^* and \hat{L} is ψ .

momentum vector can also be written as

$$\hat{L}_x = \sin i_p \sin \lambda, \quad (26)$$

$$\hat{L}_y = \cos i_p, \quad (27)$$

$$\hat{L}_z = \sin i_p \cos \lambda. \quad (28)$$

By comparing Eqs 20 to 22 with Eqs 26 to 28, it can be obtained

$$\cos I = \sin i_p \cos \lambda, \quad (29)$$

$$\tan \Omega = -\tan i_p \sin \lambda, \quad (30)$$

which allow to determine the generally unmeasurable I , Ω from i_p , λ which, instead, are observable. It can also be noted that the angle ψ between the stellar angular momentum S and the planetary orbital angular momentum L can be computed from Eqs 23 to 28 as

$$\hat{S} \cdot \hat{L} = \cos i_p \cos i^* + \sin i_p \sin i^* \cos \lambda, \quad (31)$$

in agreement with, e.g., Fabrycky & Winn (2009); Iorio (2011b). Incidentally, Equation 31, along with an analogous one which could be straightforwardly obtained from Eqs 20 to 25, explicitly shows that the node precession cannot be generally proportional to $\cos \psi$, as previously remarked in Section 2.

4 CONSTRAINING THE STELLAR SPIN AXIS

Generally speaking, while the magnitude of the classical precessions driven by the star's oblateness is at the $\approx \text{deg yr}^{-1}$ level, the relativistic gravitomagnetic ones about three orders of magnitude smaller. Despite this discrepancy, if, on the one hand, the current

state-of-the-art in the orbital determination of WASP-33 b (Johnson et al. 2015), based on data records about six years long, does not yet allow for a measurement of the relativistic effects, on the other hand, they might exceed the measurability threshold in a not so distant future. Indeed, they are just $\approx 4 - 8$ times smaller than the present-day errors, which amount to $\approx 2 - 8 \times 10^{-2} \text{ deg yr}^{-1}$ (Johnson et al. 2015) for the node.

In the following, we will reasonably assume that the measured orbital precessions of WASP-33 b are entirely due to the star's oblateness. This will allow us to put much tighter constraints on either i^* and J_2^* . Our approach is as follows. The lucky availability of the measurements of both i_p and λ at two different epochs some years apart leads to the calculation of the unobservable orbital parameters Ω , I from Eqs 29 to 30 at the same epochs. Thus, it is straightforward to compute the average rates of change $\dot{\Omega}_{\text{exp}}$, \dot{I}_{exp} for them by simply taking the ratios of the differences $\Delta \Omega$, ΔI of their values at the measurement's epochs to the time span, which in our case is $\Delta t = 6 \text{ yr}$. Our results are in Table 1. Eqs 8 to 9 provide us with an accurate mathematical model of the oblateness-driven precessions which, in view of its generality, can be straightforwardly applied to the present case. They can be viewed as two functions of the two independent variables i^* , J_2^* . By allowing them to vary within their physically admissible ranges (Iorio 2011b), it is possible to equate $\dot{\Omega}_{J_2^*}$, $\dot{I}_{J_2^*}$ to $\dot{\Omega}_{\text{exp}}$, \dot{I}_{exp} by obtaining certain stripes in the $\{i^*, J_2^*\}$ plane whose widths are fixed by the experimental ranges of the observationally determined precessions quoted in Table 1. If our model is correct and if it describes adequately the empirical results, the two stripes must overlap somewhere in the considered portion of the $\{i^*, J_2^*\}$ plane by determining an allowed region of admissible values for the inclination of the stellar spin axis to the line of sight and the star's dimensionless quadrupole mass moment. It is just the case, as depicted in Figure 2. From it, it turns that

$$i^* = 37.8^{+10.1}_{-10.8} \text{ deg}, \quad (32)$$

Table 1. Measured and derived parameters for the WASP-33 system according to Table 1 of Johnson et al. (2015) and the present study. Our values for Ω were inferred by calculating Equation 30 with the measured values of the orbital inclination i_p and of the sky-projected spin-orbit misalignment angle λ by Johnson et al. (2015), while the errors were found by numerically determining the maxima and minima of Equation 30 thought as a function of i_p , λ varying in the rectangle delimited by their measurement errors as per Table 1 of Johnson et al. (2015). The same procedure was adopted for the errors in $\dot{\Omega}_{\text{exp}}$, assumed as a function of Ω^{2008} , Ω^{2015} varying in the rectangle determined by the errors in them previously calculated.

Parameter	(Johnson et al. 2015)	This study
i_p^{2008}	$86.61_{-0.17}^{+0.46}$ deg	–
i_p^{2015}	$88.695_{-0.029}^{+0.031}$ deg	–
λ^{2008}	$-110.06_{-0.47}^{+0.49}$ deg	–
λ^{2015}	$-112.93_{-0.21}^{+0.23}$ deg	–
Ω^{2008}	$86.39_{-0.18}^{+0.49}$ deg	$86.392_{-0.192}^{+0.497}$ deg
Ω^{2015}	$88.584_{-0.032}^{+0.034} 0.014$ deg	$88.583_{-0.034}^{+0.040}$ deg
$\dot{\Omega}_{\text{exp}}$	$0.373_{-0.083}^{+0.031}$ deg yr $^{-1}$	$0.365_{-0.088}^{+0.039}$ deg yr $^{-1}$
I^{2008}	–	$110.023_{-0.403}^{+0.478}$ deg
I^{2015}	–	$112.924_{-0.660}^{+0.210}$ deg
\dot{I}_{exp}	–	$0.483_{-0.189}^{+0.102}$ deg yr $^{-1}$
J_2^*	$[0.54, 3.5] \times 10^{-2}$	$(2.1_{-0.8}^{+0.3}) \times 10^{-4}$
i^*	$[11.22, 168.77]$ deg	$37.85_{-11.08}^{+17.15}$ deg
ψ^{2008}	–	$99.4_{-3.9}^{+5.5}$ deg
ψ^{2015}	–	$102.7_{-3.9}^{+5.2}$ deg
$\dot{\psi}_{\text{exp}}$	–	$0.506_{-1.58}^{+1.52}$ deg yr $^{-1}$

$$J_2^* = (2.1_{-0.8}^{+0.5}) \times 10^{-4}. \quad (33)$$

As a consequence, the angle between the orbital plane and the stellar equator and its precession are as reported in Table 1.

As a further check of the validity of our approach, we use our findings to predict the rate of change of the impact parameter b in order to compare it with the measured value reported in Johnson et al. (2015). From its definition

$$b = \left(\frac{a}{R_{\star}} \right) \cos i_p, \quad (34)$$

valid for a circular orbit, and Eqs 21-27, it is possible to calculate its rate as

$$\dot{b} = \left(\frac{a}{R_{\star}} \right) (\sin I \sin \Omega \dot{\Omega} - \cos I \cos \Omega \dot{I}). \quad (35)$$

By computing Equation 36 with the values of Table 1, one gets

$$\dot{b}_{J_2^*} = 0.0230_{-0.0019}^{+0.0020} \text{ deg yr}^{-1}. \quad (36)$$

Up to an unessential sign convention, Equation 36 agrees with the value directly measured by Johnson et al. (2015) with Doppler tomography.

An opportunity to apply the present method to another exoplanet should be offered in the next future by Kepler-13 Ab (KOI-13.01) (Szabó et al. 2012; Shporer et al. 2014; Johnson et al. 2014;

Masuda 2015), whose orbital precession should be measurable via Doppler tomography by 2017.

5 SUMMARY AND CONCLUSIONS

The use of a general model of the orbital precessions caused by the primary's oblateness, valid for arbitrary orbital geometries and spatial orientations of the body's symmetry axis, applied to recent phenomenological measurements of some planetary orbital parameters of WASP-33 *b*, taken at different epochs some years apart, allowed us to tightly constrain the inclination i^* of the spin S of WASP-33 to the line of sight and its dimensionless quadrupole mass moment J_2^* .

By comparing our theoretical orbital rates of change to the observationally determined ones, we obtained $i^* = 37.8_{-10.8}^{+10.1}$ deg, $J_2^* = (2.1_{-0.8}^{+0.5}) \times 10^{-4}$. Furthermore, the angle between the stellar and orbital angular momenta at different epochs is $\psi^{2008} = 99.4_{-3.9}^{+5.5}$ deg, $\psi^{2015} = 102.7_{-3.9}^{+5.2}$ deg. Thus, it varies at a rate $\dot{\psi} = 0.506_{-1.58}^{+1.52}$ deg yr $^{-1}$.

In view of the fact that WASP-33 *b* should transit its host star until 2062 or so and of the likely improvements in the measurement accuracy over the years, such an extrasolar planet will prove a very useful tool for an increasingly accurate characterization of the key physical and geometrical parameters of its parent star via its orbital

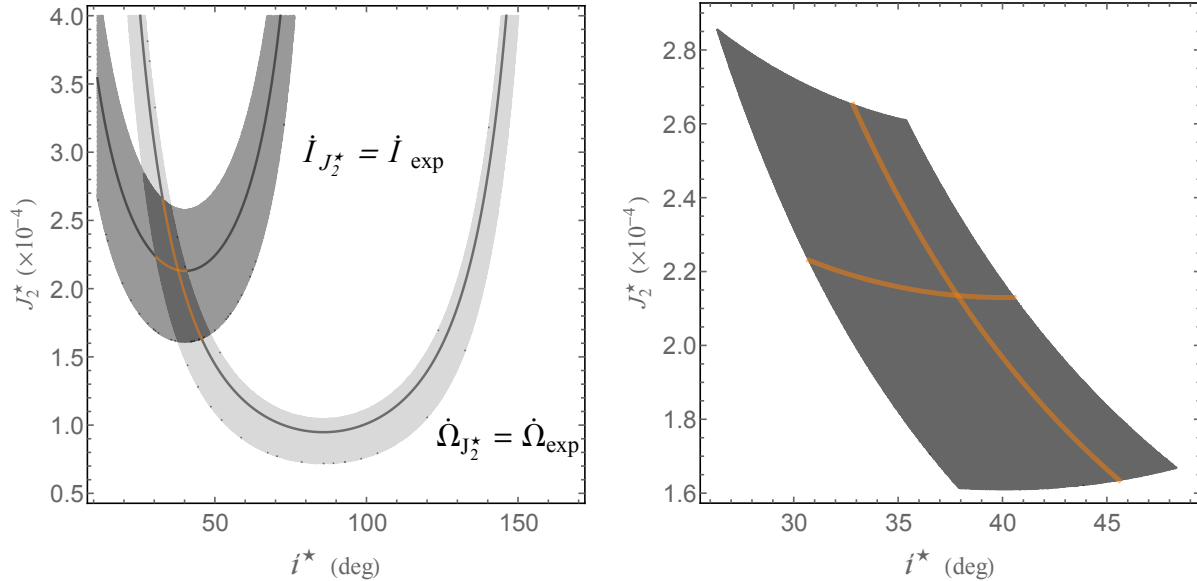


Figure 2. The darkest region in the plot is the experimentally allowed area in the $\{i^*, J_2^*\}$ plane, which is enlarged in the right panel. It is determined by the overlapping of the permitted shaded stripes set by the precessions of the node Ω and the orbital inclination to the apparent equatorial plane I . We assumed that the experimental precessions $\dot{\Omega}_{\text{exp}}$, \dot{I}_{exp} are entirely due to the stellar oblateness J_2^* , within the experimental errors. For $\dot{\Omega}_{J_2^*}$, $\dot{I}_{J_2^*}$, we used the mathematical model of Eqs 8 to 9 calculated with the values quoted in Table 1. The curves inside the shaded areas correspond to the best estimates for $\dot{\Omega}_{\text{exp}}$, \dot{I}_{exp} ; their intersection is given by $i^* = 37.85$ deg, $J_2^* = 2.13344 \times 10^{-4}$.

dynamics. Moreover, also the determination of the Lense-Thirring effect, whose predicted size is currently just one order of magnitude smaller than the present-day accuracy level in determining the planetary orbital precessions, may become a realistic target to be pursued over the next decades.

Finally, in view of its generality, our approach can be straightforwardly applied to any other exoplanetary system, already known or still to be discovered, for which at least the same parameters as of WASP-33 b are or will become accessible to the observation. A promising candidate, whose orbital precession should be measurable via Doppler tomography by 2017, is Kepler-13 Ab. Moreover, in principle, also the periastron, if phenomenologically measurable at different epochs as in the present case, can become a further mean to investigate the characteristics of highly eccentric exoplanetary systems-and to test general relativity as well-along the guidelines illustrated here.

ACKNOWLEDGEMENTS

I would like to thank M. C. Johnson for useful correspondence and clarifications.

REFERENCES

Adams F. C., Laughlin G., 2006a, *Astrophys. J.*, 649, 992
 Adams F. C., Laughlin G., 2006b, *Astrophys. J.*, 649, 1004
 Adams F. C., Laughlin G., 2006c, *Int. J. Mod. Phys. D*, 15, 2133
 Angélin R., Saha P., Merritt D., 2010, *Astrophys. J.*, 720, 1303
 Barnes J. W., van Eyken J. C., Jackson B. K., Ciardi D. R., Fortney J. J., 2013, *Astrophys. J.*, 774, 53

Bertotti B., Farinella P., Vokrouhlick D., 2003, *Physics of the Solar System - Dynamics and Evolution, Space Physics, and Space-time Structure*. Kluwer, Dordrecht
 Burgay M. et al., 2003, *Nature*, 426, 531
 Collier Cameron A. et al., 2010, *Mon. Not. Roy. Astron. Soc.*, 407, 507
 Cook G. E., 1962, *Rep. Prog. Phys.*, 25, 63
 Cugusi L., Proverbio E., 1978, *Astron. Astrophys.*, 69, 321
 Damiani C., Rozelot J. P., Lefebvre S., Kilcik A., Kosovichev A. G., 2011, *J. Atm. and Solar-Terrestrial Phys.*, 73, 241
 Einstein A., 1915, *Sitzungsber. Preuss. Akad. Wiss.*, 47, 831
 Fabrycky D. C., Winn J. N., 2009, *Astrophys. J.*, 696, 1230
 Ghez A. M. et al., 2008, *Astrophys. J.*, 689, 1044
 Gillessen S., Eisenhauer F., Trippe S., Alexander T., Genzel R., Martins F., Ott T., 2009, *Astrophys. J.*, 692, 1075
 Han E., Wang S. X., Wright J. T., Feng Y. K., Zhao M., Fakhouri O., Brown J. I., Hancock C., 2014, *Publ. Astron. Soc. Pac.*, 126, 827
 Haranas I., Ragos O., Mioc V., 2011, *Astrophys. Space Sci.*, 332, 107
 Herbst W., Mundt R., 2005, *Astrophys. J.*, 633, 967
 Heyl J. S., Gladman B. J., 2007, *Mon. Not. Roy. Astron. Soc.*, 377, 1511
 Howard A. W., 2013, *Science*, 340, 572
 Hulse R. A., Taylor J. H., 1975, *Astrophys. J. Lett.*, 195, L51
 Iorio L., 2006, *New Astron.*, 11, 490
 Iorio L., 2011a, *Mon. Not. Roy. Astron. Soc.*, 411, 167
 Iorio L., 2011b, *Astrophys. Space Sci.*, 331, 485
 Iorio L., 2011c, *Phys. Rev. D*, 84, 124001
 Iorio L., 2012, *General Relativity and Gravitation*, 44, 719
 Jackson S., MacGregor K. B., Skumanich A., 2005, *Astrophys. J. Suppl.*, 156, 245
 Johnson M. C., Cochran W. D., Albrecht S., Dodson-Robinson

S. E., Winn J. N., Gullikson K., 2014, *Astrophys. J.*, 790, 30
 Johnson M. C., Cochran W. D., Collier Cameron A., Bayliss D.,
 2015, ArXiv e-prints
 Jordán A., Bakos G. Á., 2008, *Astrophys. J.*, 685, 543
 King-Hele D. G., 1962, *Geophys. J. Int.*, 6, 270
 Kozai Y., 1961, *Astron. J.*, 66, 8
 Kramer M. et al., 2006, *Science*, 314, 97
 Lapaz L., 1954, *Publ. Astron. Soc. Pac.*, 66, 13
 Le Verrier U., 1859, *Cr. Hebd. Acad. Sci.*, 49, 379
 Lense J., Thirring H., 1918, *Phys Z.*, 19, 156
 Li L.-S., 2012, *Astrophys. Space Sci.*, 341, 323
 Lucchesi D. M., Peron R., 2010, *Phys. Rev. Lett.*, 105, 231103
 Lucchesi D. M., Peron R., 2014, *Phys. Rev. D*, 89, 082002
 Lyne A. G. et al., 2004, *Science*, 303, 1153
 Masuda K., 2015, *Astrophys. J.*, 805, 28
 Pál A., Kocsis B., 2008, *Mon. Not. Roy. Astron. Soc.*, 389, 191
 Perryman M., 2014, *The Exoplanet Handbook*. Cambridge, UK:
 Cambridge University Press
 Queloz D., Eggenberger A., Mayor M., Perrier C., Beuzit J. L.,
 Naef D., Sivan J. P., Udry S., 2000, *Astron. Astrophys.*, 359, L13
 Ragozzine D., Wolf A. S., 2009, *Astrophys. J.*, 698, 1778
 Rozelot J.-P., Damiani C., 2011, *Eur. Phys. J. H.*, 36, 407
 Rozelot J. P., Damiani C., Pireaux S., 2009, *Astrophys. J.*, 703,
 1791
 Rozelot J. P., Fazal Z., 2013, *Sol. Phys.*, 287, 161
 Shporer A. et al., 2014, *Astrophys. J.*, 788, 92
 Szabó G. M., Pál A., Derekas A., Simon A. E., Szalai T., Kiss
 L. L., 2012, *Mon. Not. Roy. Astron. Soc.*, 421, L122
 Tarafdar S. P., Vardya M. S., 1971, *Astrophys. Space Sci.*, 13, 234
 Vigneron C., Mangeney A., Catala C., Schatzman E., 1990, *Sol.
 Phys.*, 128, 287
 Vrbik J., 2005, *Celestial Mechanics and Dynamical Astronomy*,
 91, 217
 Wolff S., Simon T., 1997, *Publ. Astron. Soc. Pac.*, 109, 759
 Wolff S. C., Edwards S., Preston G. W., 1982, *Astrophys. J.*, 252,
 322
 Xie Y., Deng X.-M., 2014, *Mon. Not. Roy. Astron. Soc.*, 438,
 1832
 Zhang F., Lu Y., Yu Q., 2015, *Astrophys. J.*, 809, 127
 Zhao S.-S., Xie Y., 2013, *Res. Astron. Astrophys.*, 13, 1231